Materials Today Advances 16 (2022) 100288

Contents lists available at ScienceDirect

Materials Today Advances

journal homepage: www.journals.elsevier.com/materials-today-advances/

# Alkaline-responsive polydiacetylene-peptide hydrogel for pH-sensing and on-demand antimicrobial release

Weike Chen [a], Shan Hazoor [a], Ryan Madigan [a], Ashley A. Adones [a], Uday K. Chintapula [b], Kytai T. Nguyen [b], Liping Tang [b], Frank W. Foss Jr. [a], He Dong [a, *]

[a] Department of Chemistry and Biochemistry, The University of Texas at Arlington, Arlington, TX, 76019, USA
[b] Department of Bioengineering, The University of Texas at Arlington, Arlington, TX, 76019, USA

ARTICLE INFO

*Article history:*
Received 18 July 2022
Received in revised form
18 August 2022
Accepted 21 August 2022
Available online 5 September 2022

*Keywords:*
Hydrogels
Antimicrobial delivery
Colorimetric sensing
Alkaline pH
Peptide self-assembly
Polydiacetylene

ABSTRACT

Antibiotic resistance is a global public health issue, accelerated by the misuse and overuse of antibiotics. Microenvironment-targeted antimicrobial delivery is an emergent and promising strategy for selective antibiotic delivery that targets the site of infections and may reduce drug resistance. The local pH of infected tissues can be a primary target for designing materials with pH-triggered antimicrobial activity. Given the urgent need to combat bacterial infections in diseases with an elevated pH, we report on the design and synthesis of a new alkaline-responsive antimicrobial hydrogel. The gels are based on a polydiacetylene-peptide (PDA-Pep) having pH-dependent molecular and macromolecular structure and packing. Upon pH elevation, the peptide domain is deprotonated and triggers the conformational change of the PDA domain, leading to a colorimetric transition from blue to purple. Simultaneously, the deprotonation induces a gel-to-sol macroscopic phase transition of the fiber network formed in PDA-Pep hydrogels, which causes the selective release of the antimicrobial agents that are encapsulated in the gels into the infection site to kill bacteria. The translational potential of PDA-Pep hydrogels for pH-sensing and on-demand alkaline-triggered antibiotic delivery was demonstrated on inoculated pig skins. The work lays the foundation for the development of multifunctional alkaline-responsive materials in which multiple small molecule or macromolecular therapeutics can be encapsulated to achieve synergistic biological functions against a wide range of multidrug-resistant pathogens.



## 1. Introduction

Given the ever-growing public health problem posed by antibiotic resistance, there is an urgent need to advance novel antimicrobial strategies to combat drug-resistant infectious diseases. Stimuli-responsive drug delivery has the potential to provide effective treatments through releasing antibiotics at the infection sites to maximize therapeutic efficacy and minimize drug resistance [1–3]. Among various stimuli, pH has been considered as an important endogenous stimulus for the design and synthesis of pH-responsive materials to selectively deliver antibiotics at the site of infection [4,5]. In the past several decades, acid-responsive materials have been extensively explored to treat infections caused by lactic acid-producing bacteria [6–8]. However, materials that can respond to an alkaline bacterial microenvironment, for example diseases involving chronic wound infections (pH 7.2–8.9) [9,10], pancreas infections (pH 7.5–8.5) [11,12] and catheter-associated urinary tract infections (pH 7.0–8.5) [13] are still underdeveloped. From the viewpoint of both fundamental and practical materials research [14–16], there is a need to explore novel stimuli-responsive materials that can target bacterial infections associated with local pH increase. It is more beneficial to develop a system capable of both sensing/signaling and on-demand antimicrobial delivery. Such systems would greatly benefit clinical research on real-time bacterial infection imaging and antimicrobial therapy.

Inspired by the recent advances in polydiacetylene (PDA)-based biosensor design [17–22], we aim to establish a new class of alkaline-responsive hydrogels based on PDA-peptide (PDA-Pep) conjugates for colorimetric pH-sensing and antimicrobial properties. PDA-Pep is a new family of nanomaterials that are constructed through the self-assembly of diacetylene-peptide (DA-Pep) to form supramolecular nanofibers or micelles [23–27]. In particular, when nanofibers are formed, the DA components are aligned internally

* Corresponding author.
*E-mail address:* he.dong@uta.edu (H. Dong).

https://doi.org/10.1016/j.mtadv.2022.100288

along the long fiber axis of the nanofiber while the peptide moieties are flanking at the fiber-solvent interface. Upon UV irradiation, DA undergoes polymerization to form PDA with conformation-dependent chromic properties. Compared with other PDA-based materials, PDA-Pep have unique advantages regarding the control over the internal order of each molecular and macromolecular components within the nanofibers. The use of peptides provides an efficient method to tune not only the intermolecular packing within a single fiber, but also the macroscopic packing of these nanofibers to form higher-ordered dynamic assemblies. In this work, we take advantage of the dynamic nature of PDA-Pep to design and synthesize a new family of alkaline-responsive hydrogels for monitoring and signaling the alkaline microenvironment upon bacterial infection and consequently control antimicrobial characteristics.

## 2. Materials and methods

### 2.1. Materials

Reagents used to synthesize the diphenyl-diacetylene linker and DA-Pep conjugates were purchased from commercial sources and used without further treatment. TEM staining reagent, uranium acetate dihydrate, and TEM grids were purchased from Ted Pella, Inc. Methicillin-resistant *staphylococcus aureus* (ATCC 33592) was purchased from ATCC. Detailed product information is included in the SI.

### 2.2. Synthesis of diphenyldiacetylene linker (DA)

DA linker (**6**) was synthesized as depicted in the SI (Scheme 1). In general, Sonogashira cross coupling was carried out between ethyl 4-bromobezoate and trimethylsilylacetylene to acquire the aryl alkyne (**3)** with 67% yield. Deprotection of the trimethylsilyl group (TMS) was performed with $K_2CO_3$ in ethanol to get terminal alkyne (**4**) with 62% yield. Glaser coupling enabled the diacetylene functional group of the DA linker. Copper acetate monohydrate $Cu(OAc)_2 \cdot H_2O$ was effective at generating the diacetylene compound (**5**) with 80% yield. Ester hydrolysis was accomplished with $NaOH_{(aq)}$ to obtain the final product as an off-white solid in 73% yield (**6**).

### 2.3. Peptide synthesis and purification

Peptides were synthesized on a *Prelude*® peptide synthesizer using a standard Fmoc-solid phase peptide synthesis procedure, as detailed in the SI. After final Fmoc group deprotection, the resin was transferred into a rotary reaction vessel and the conjugation between the DA linker and peptide was performed in the presence of HBTU and DIPEA in DMF. After 48 h, the completion of the coupling reaction was confirmed by the Kaiser test. DA-Pep was cleaved by a cocktail of TFA/Tris/$H_2O$ (95/2.5/2.5 by volume) for 3 h. The cleavage solution was filtered, and the filtrates were collected. The resin was washed three times with neat TFA, and all filtrate solutions were combined and evaporated under airflow. The residual TFA solution was precipitated in cold diethyl ether, followed by centrifugation and washing with cold diethyl ether for three times. The crude product was dried under vacuum overnight for HPLC purification. DA-Pep was purified using a semi-prep C4 reversed-phase column with a linear gradient of water/acetonitrile (5%–95% of acetonitrile in 30 min) containing 0.05% TFA. Elution was monitored at 230 nm and 280 nm. Mass was confirmed by electrospray ionization mass spectrometry. Calculated mass $[M+2H]^{2+}$ for DA-Pep (peptide sequence: GQFQFEGGGLPRDA): 1605.10 and experimental mass $[M+2H]^{2+}$: 1605.40. Calculated mass $[M+2H]^{2+}$ for DA-Pep (peptide sequence: GQFEGGGLPRDA): 1329.30 and experimental mass $[M+2H]^{2+}$: 1329.55. Calculated mass $[M+2H]^{2+}$ for DA-Pep (peptide sequence: GSFEGGGLPRDA): 1288.24 and experimental mass $[M+2H]^{2+}$: 1288.80. Calculated mass $[M+2H]^{2+}$ for DA-Pep (peptide sequence: GQIEGGGLPRDA): 1295.28 and experimental mass $[M+2H]^{2+}$: 1295.50. Calculated mass $[M+2H]^{2+}$ for peptide without DA (peptide sequence: GQFEGGGLPRDA): 622.17 and experimental mass $[M+2H]^{2+}$: 622.38. Calculated mass $[M+3H]^{3+}$for $K_8(QF)_6K_8$: 1254.00 and experimental mass $[M+3H]^{3+}$: 1255.00.

### 2.4. Preparation of PDA-Pep hydrogels

The DA-Pep hydrogel was first prepared by dissolving lyophilized powder directly in MES buffer (pH 5.5) to reach a final concentration at 10 mg/mL. The hydrogel was polymerized to form PDA-Pep through UV irradiation with a hand-held UV lamp (254 nm, 6 W) for 1 h with a distance of approximately one cm. PDA-Pep (Van) hydrogels were prepared with the same procedure but using MES buffer (pH 5.5) containing pre-dissolved vancomycin at 10 μM. PDA-Pep (AMP) hydrogels were prepared with the same procedure but using MES buffer (pH 5.5) containing pre-dissolved AMP at 20 μM.

### 2.5. Transition pH determination by UV–vis spectroscopy

The samples were prepared by dilution of the PDA-Pep hydrogel to a concentration at 150 μM in various Britton–Robinson buffer (20 mM) with pH at 5.5, 6.0, 6.5, 6.8, 7.3, 7.5, 8.0 and 8.5. The UV–vis spectra were collected from 400 to 800 nm at room temperature using a 1 mm cuvette. The absorbance ratio data of $A_{566}/A_{652}$ was fitted into the sigmoidal Boltzmann equation implemented in OriginPro 9.0.

### 2.6. Bacterial killing efficiency in culture

*MRSA* was cultured in MHB medium under constant shaking at 100 rpm at 37 °C to reach the mid-exponential growth phase. The bacterial solution was plated on an agar plate for colony forming unit (CFU) counting. Bacterial suspensions were diluted to approximately $1 \times 10^5$ CFU/mL in various MHB medium at pH 5.5, 6.5, 7.5, and 8.5. PDA-Pep, PDA-Pep (Van) and PDA-Pep (AMP) hydrogels were prepared in MES buffer (pH 5.5) by UV irradiation with a concentration of 10 mg/mL. 50 μL of bacterial suspensions at different pHs were loaded on top of the hydrogels (50 μL) and each sample was prepared in duplicates. Upon 4 h of incubation, both the gels and bacterial suspensions were quickly transferred to a MHB medium followed by 10-fold serial dilution for plating counting of viable bacteria. Bacterial killing efficiency was determined as the ratio of the viable bacteria in cultures treated with PDA-Pep (Van) or PDA-Pep (AMP) gels to that of the PDA-Pep gel group.

### 2.7. Bacterial killing efficiency on pig skins

*MRSA* cultures were prepared in MHB media at pH 5.5, 6.5, 7.5, and 8.5. Pig skins were treated with 70% of ethanol solution before bacterial inoculation. 30 μL of PDA-Pep or PDA-Pep (Van) hydrogels were applied on top of the inoculation sites and incubated at 37 °C for up to 2 h. Visual color changes were recorded at 5 min, 0.5 h, 1 h, and 2 h showing alkalinity-responsive blue-to-purple color change.

After 2 h, pig skins were thoroughly washed with MHB medium and solutions were collected and subject to serial dilution and plate counting. The killing efficiency was calculated as the ratio of the viable bacteria on pig skins treated with PDA-Pep (Van) gel to that of the PDA-Pep gel group. Each sample was prepared in duplicates.

## 3. Results and discussion

### 3.1. Design of alkaline-responsive PDA-Pep hydrogels

Scheme 1 shows the chemical structure of DA-Pep and its dynamic self-assembly and disassembly process with pH. DA-Pep contains an internal aromatic diphenyl-diacetylene linker which is attached to a glutamic acid-containing oligopeptide bearing a bacterial targeting ligand at both ends (Scheme 1A). Based on the design principle, self-assembly of DA-Pep occurs under an acidic condition when the charge on the oligopeptide is neutralized, leading to supramolecular nanofibers with internally aligned DA groups (Scheme 1B). At a high concentration of DA-Pep, macroscopic hydrogels, which consist of physically crosslinked supramolecular nanofibers can be formulated. Upon UV irradiation, DA is polymerized to form PDA showing a characteristic blue color. As the local pH increases, glutamic acids are deprotonated and therefore electrostatic repulsion is generated among the oligopeptides. There are two levels of structural control with pH increase. On the molecular level, the electrostatic repulsion among the peptide domains will change the packing and conformation of PDA within a single nanofiber. The conformational change of PDA is known to induce a colorimetric transition from blue to red or purple and therefore can provide visual and spectroscopic read-out for the local pH change (Scheme 1B). On the macroscopic level, the hydrogel is likely to be disrupted as a result of the repulsive interaction between individual fibers upon pH increase. A gel-to-sol transition is expected as the solution becomes alkaline. It is worth noting that small molecule antibiotics and/or antimicrobial peptides (AMPs) can be readily incorporated into the hydrogels during the formulation process and are subject to release upon gel-to-sol transition as the local pH increases.

### 3.2. Hydrogel formation

The synthetic procedures and purification steps for the DA-linker and DA-Pep were shown in the SI (**SI**, **Scheme-1**, Figs. S1–1 to **S1-9** and Fig. S2). A small library of DA-Pep was synthesized and tested for their gelation capability under the acidic condition (pH 5.5) by the tube inversion method (Fig. S3). Initially, we started with a sequence containing a binary hydrophilic-hydrophobic residue repeating unit of QFQF in the peptide domain (Q: glutamine, F: phenylalanine), which is known to drive β-sheet packing [28,29]. However, as shown in Fig. S3A, this construct failed to form gels, nor did it polymerize. Further increasing the number of QF repeating units was ineffective to promote gelation, rather it caused precipitates due to phase separation upon self-assembly (data not shown). On the contrary, DA-Pep containing a single QF motif was found to form gel which can be further polymerized as shown by the appearance of a blue color upon UV irradiation (Fig. S3B). The results suggest an unstructured oligopeptide is more favorable for the self-assembly process in which a delicate balance can be achieved between the π-π stacking among the DA domains and the intermolecular hydrogen packing among the peptide domains. Peptides with an intrinsic secondary structural propensity are likely to compromise the internal alignment of the DA domain needed to

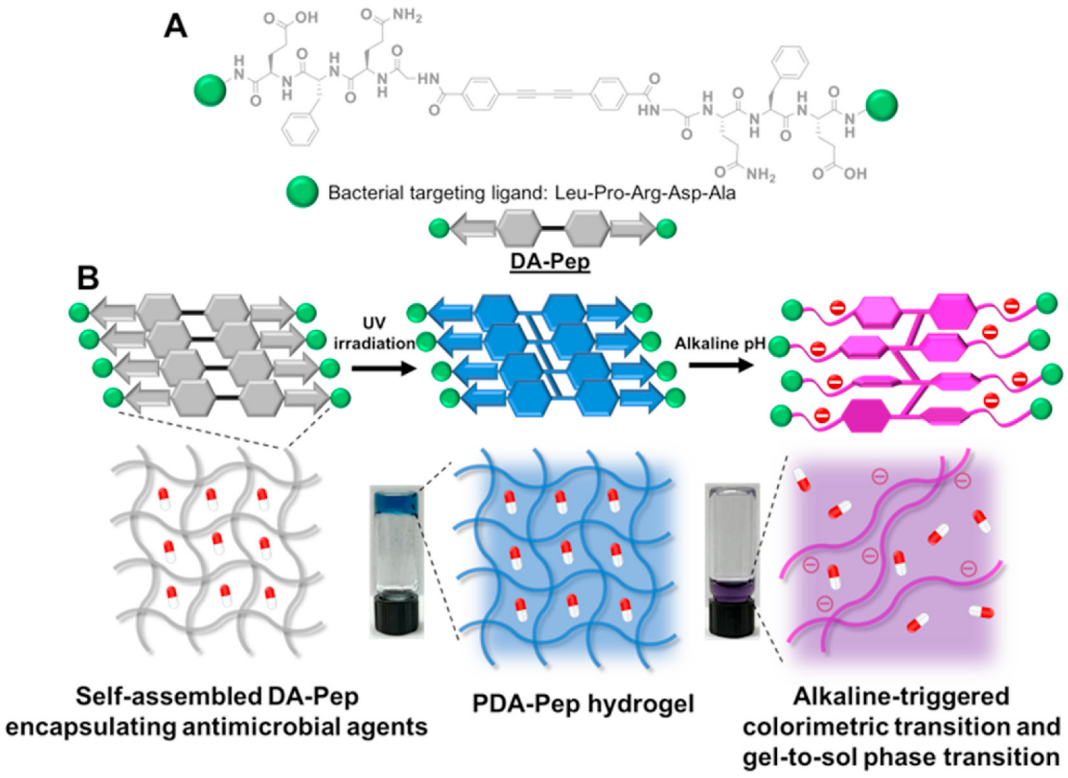


**Scheme 1.** Illustration of the chemical design of PDA-Pep hydrogels that undergo alkaline-triggered blue-to-purple colorimetric transition with simultaneous gel-to-sol phase transition for antibiotic release. (**A**) Chemical structure of DA-Pep conjugate. (**B**) Illustration of self-assembled DA-Pep (in grey) that forms an elongated nanofiber and the formation of PDA-Pep hydrogel that appear in blue upon UV irradiation. The PDA-Pep became charged under the alkaline condition, which led to a conformational change of the PDA domain and a blue-to-purple colorimetric transition. The electrostatic repulsion induces a gel-to-sol transition and consequently antimicrobial release.

form ordered supramolecular nanofibers and further macroscopic hydrogelation. It was also found that substitution of glutamine with serine completely inhibited gelation although polymerization still occurred (Fig. S3C). Substitution of phenylalanine with aliphatic isoleucine did not affect gelation (Fig. S3D); however, the color transition upon pH increase was less sensitive compared to that of DA-Pep with a QF sequence (Fig. S3E). Notably, the pH-dependent gelation and colorimetric transition were reversible as shown in Fig. S3F. Given the initial screening result, we selected DA-Pep with the sequence of QF to construct alkaline-responsive hydrogels and investigate its alkaline-triggered colorimetric transition and antibiotic release.

### 3.3. pH-dependent colorimetric transition and gel-to-sol transition

We are primarily interested in the pH range from 5.5 to 8.5 due to their implication toward bacterial infections in several diseases, especially those found in wound healing. Gels were first prepared in a MES buffer at pH 5.5 and the pH was adjusted using sodium hydroxide to the desired values at 6.5, 7.5 and 8.5. As shown in Fig. 1A, at pH 5.5, DA-Pep formed a stable self-supporting hydrogel which appeared blue upon UV-initiated polymerization. With the increase of pH, glutamic acids became deprotonated, and a net negative charge was built on each fibril to induce electrostatic repulsion between individual fibrils. The inter-fibril repulsion eventually disrupted the physical crosslinking in the hydrogel and a gel-to-sol transition was observed accordingly. This macroscopic structural change upon gel-to-sol transition was confirmed by transmission electron microscopy (TEM) showing a densely packed fibrous network at pH 5.5 and gradually reduced to dispersed fibers at pH 8.5 (Fig. S4). Notably, the gel-to-sol phase transition was accompanied by a blue-to-purple colorimetric transition, which was presumably caused by the conformational change of the PDA moieties within a single nanofiber. To further quantify the colorimetric transition, which can be potentially used as a diagnostic tool for monitoring the alkalinity of bacterial microenvironment, UV–vis spectroscopy was used to examine the conformation-dependent absorption at various pH values. As shown in Fig. S5, PDA-Pep showed a major absorption peak at 652 nm with a vibronic shoulder at 596 nm at all pHs up to 6.8. Consistent with literature reports [30–32], the peak at 652 nm is a signature absorption for PDA conformation that results in a visible blue color. As the solution became alkaline and a blue-to-purple colorimetric transition occurred, the absorption at 652 nm was dramatically reduced and a single broad peak at 566 nm was predominant, suggesting a conformational change of PDA. The ratio of the absorption at 566 nm and 652 nm represents the relative contribution of each chromatic solution component that is associated with different PDA conformations. Fitting the ratio of ($A_{566}/A_{652}$) to a modified Boltzmann sigmoidal function allowed the estimation of the transition pH, i.e. the first derivative of the sigmoidal curve, which was at 7.3 (Fig. 1B). The sensitivity of the colorimetric assay was further quantified based on the ratio of the UV–Vis absorption at 566 nm and the overall absorption values at both 566 nm and 652 nm, i.e. $A_{566}/(A_{566}+A_{652})$. The results showed that PDA-Pep was highly sensitive to pH change with 81% colorimetric response at pH 8.5 and 70% at pH 7.5 versus 35% at pH 6.5 and 30% at pH 5.5 (Fig. 1C).

To gain deeper insights into the molecular mechanism for the gel-to-sol transition and in particular colorimetric transition of PDA-Pep, we performed circular dichroism (CD) spectroscopic measurement, which provides information about molecular conformation of both peptides and PDA at different pH values. There are two distinct chiral absorption regions on the CD spectrum. As shown in Fig. 2, in the far UV region (200 nm–280 nm), a peak shift was observed from 214 nm to ~200 nm as the solution became basic. The result suggests that the peptide moiety adopted a predominant β-sheet structure under the acidic condition and unfolded to a random coil under a neutral or alkaline condition. Notably, the peptide alone without DA conjugation formed a random coil structure across all pH ranges (Fig. S6) and TEM did not reveal defined fibrous structures (Fig. S7). The black dots observed in Fig. S7 are simply the aggregates of peptide without the DA linker. This could occur due to the drying effect during TEM sample preparation. These results suggest the important role of the DA in promoting the molecular and supramolecular packing of DA-Pep to form supramolecular nanofibers in which the peptides form an ordered molecular secondary structure through intermolecular hydrogen bonding. In the middle and near UV region (280 nm–400 nm), a strong chiral absorption was observed under

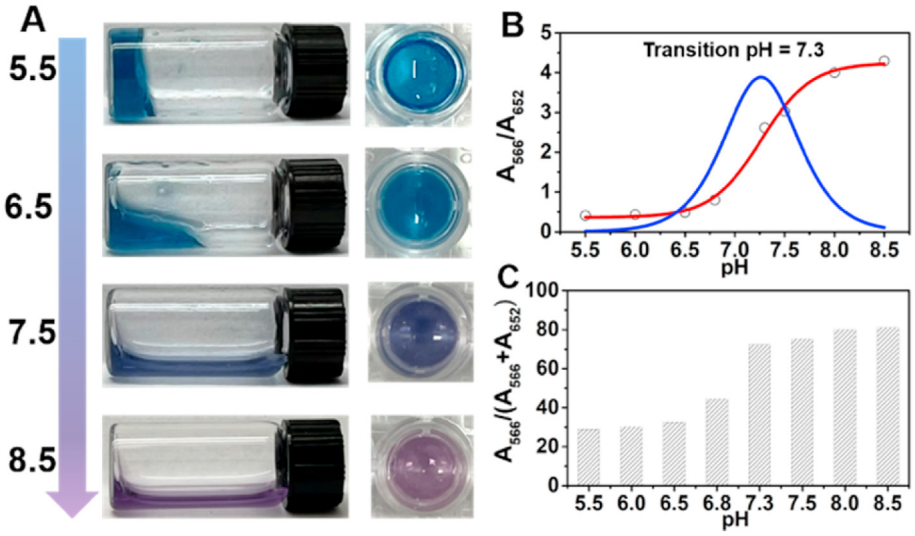


**Fig. 1.** **(A)** pH-dependent gel and sol phase of PDA-Pep and their optical images showing an alkaline triggered blue-to-purple colorimetric transition. PDA-Pep concentration: 10 mg/mL. (**B**) Boltzmann sigmoidal fitting and first derivative of the absorbance ratio of $A_{566}/A_{652}$ as a function of pH to determine the colorimetric transition pH. (**C**) Colorimetric response of PDA-Pep at various pH values. PDA-Pep concentration: 100 μM.

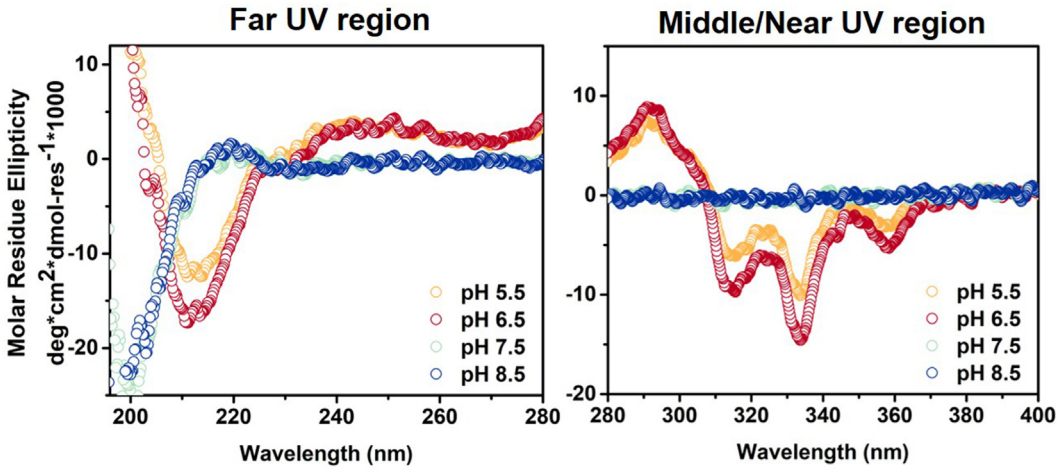


**Fig. 2.** CD spectra of PDA-Pep at different pH values. The far UV region (left) shows the secondary structure of the peptide domain and the middle and near UV region (right) shows the chiral absorption of the PDA domain. PDA-Pep concentration: 100 μM.

the acidic condition (Fig. 2). It has been reported that macromolecular self-assembly could facilitate supramolecular chirality transfer from the chiral groups to an achiral moiety [33,34]. For the PDA-Pep, the Cotton effect shown between 300 nm and 380 nm is presumably attributed to such chirality transfer from the peptide domain to the PDA that are both organized within the supramolecular nanofibers. The chiral absorption wavelengths on the CD spectrum match well with UV—vis absorption of the PDA moiety (Fig. S5), further confirming the supramolecular chiral packing of the PDA upon self-assembly. As pH increases, the Cotton effect in the near UV region was diminished, suggesting a change of molecular conformation, and packing of the PDA domain. As discussed above, this conformation change is likely caused by the electrostatic repulsion among peptides that are deprotonated upon pH increase. The electrostatic repulsion disrupts ideal hydrophobic and π-π interactions within the PDA domain, and eventually drives a conformational change of PDA as charges continue to build up on the peptides, yielding a red-shifted, less conjugated PDA chromophore.

### 3.4. Alkaline-triggered antimicrobial release from PDA-Pep hydrogels

Antimicrobial agents, such as vancomycin (Van) or synthetic AMPs can be readily encapsulated into PDA-Pep hydrogels and released upon gel-to-sol transition to achieve controlled antimicrobial release. Notably, we used a custom-designed cationic AMP with the sequence of $K_8(QF)_6K_8$ in which the subscript indicates the number of the repeating units for lysine and the binary QF motif. MES buffer (pH 5.5) containing Van or AMP was used to dissolve DA-Pep powder. Gelation immediately occurred and was subject to UV polymerization to form PDA-Pep hydrogels that appeared blue. We monitored the release of Van and AMPs from the hydrogels to the aqueous buffer which was placed on top of the gels over time. As shown in Fig. S8, at pH 7.5, PDA-Pep hydrogel showed a time-dependent release profile with nearly 90% of Van and 100% of AMP were released over a 4 h incubation period. At pH 8.5, nearly 100% of Van and AMP were released at the end of 4 h incubation. At pH 5.5, less than 10% of antimicrobial agents were released from gels. The results suggest the great potential of these PDA-Pep hydrogels as smart antimicrobial materials capable of on-demand antimicrobial release upon the increase of local microenvironment pH.

### 3.5. Alkaline-triggered antimicrobial activity of PDA-Pep hydrogels

The ability of PDA-Pep hydrogels to undergo on-demand, alkaline-triggered antimicrobial delivery to kill or inhibit the growth of bacteria was further evaluated. Methicillin-resistant staphylococcus aureus (*MRSA*) was selected for bacterial killing assay study. *MRSA* has a high expression of sortase receptors on its bacterial cell membrane [35]. Therefore, we added an additional oligopeptide ligand (with the sequence of LPRDA) that can recognize the sortase receptors on *MRSA* [36]. On the other hand, for future *in vivo* therapeutic study, the use of a bacteria-targeted peptide can help recruit and capture targeted pathogenic bacteria and localize the killing effects. A general experimental set-up for the antimicrobial assay is shown in Fig. 3A. MES buffer (pH 5.5) containing Van or AMP was used to dissolve DA-Pep powder to form hydrogels. The gels were subject to UV polymerization to form PDA-Pep hydrogels that appeared in blue color (**step 1**). The gels were prepared with a final concentration of 10 mg/mL and used for all the following studies. *MRSA* culture at varying pH values was loaded on top of the PDA-Pep gels (**step 2**). Visual inspection of the color change was followed during the incubation time (**step 3**) and bacterial killing efficiency was determined through plate counting at the end of 4 h of incubation period (**step 4**). Fig. 3B and **C** shows the optical images of Van-encapsulated PDA-Pep gels, denoted as PDA-Pep (Van) and AMP-encapsulated PDA-Pep denoted as PDA-Pep (AMP) incubated with acidic or alkaline bacterial culture at 5 min and 4 h time point. It was found that PDA-Pep (Van) and PDA-Pep (AMP) hydrogels incubated with an acidic bacterial culture maintained the original blue color after 4 h of incubation. On the contrary, the PDA-Pep (Van) and PDA-Pep (AMP) hydrogels exhibited a blue-to-violet colorimetric transition upon incubation with bacterial cultures at pH 7.5 and further changed to purple at pH 8.5. As shown earlier, the pH-dependent colorimetric transition occured synergistically with a gel-to-sol phase transition which provides an opportunity for on-demand delivery of antimicrobials at the site of bacterial infection under the alkaline conditions. Bacterial killing efficiency of PDA-Pep (Van) and PDA-Pep (AMP) hydrogels against *MRSA* at different pH values was determined by plate counting of the viable

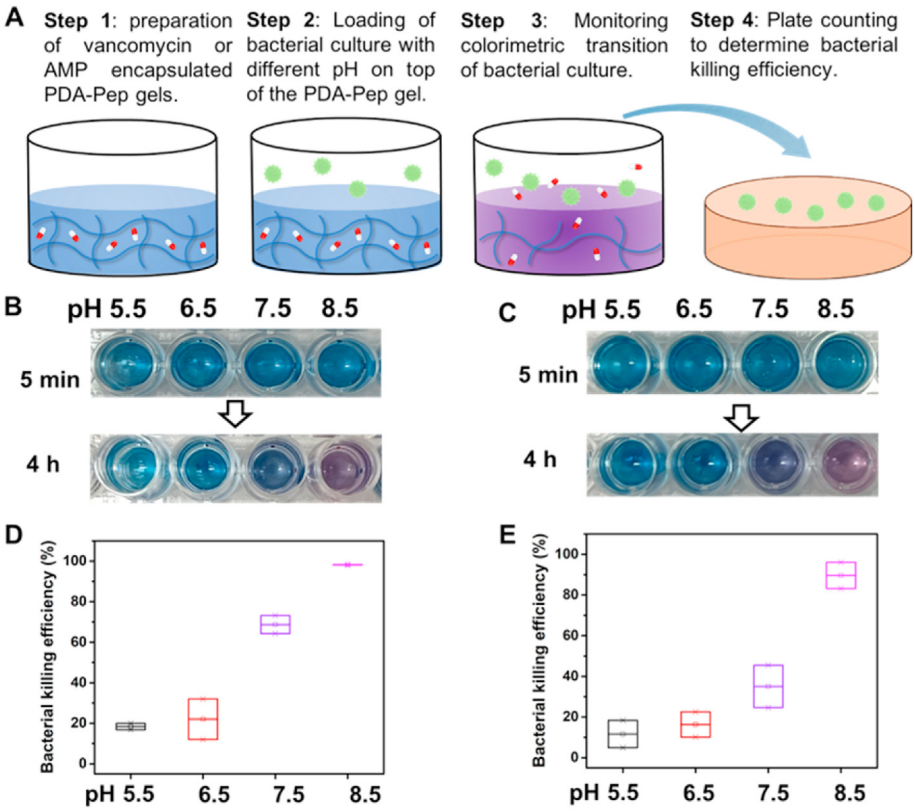


**Fig. 3.** (**A**) Experimental set up for the evaluation of alkaline-triggered antimicrobial release and their bacterial killing efficiency. Colorimetric transition of (**B**) PDA-Pep (Van) and (**C**) PDA-Pep (AMP) upon incubation with bacterial cultures at different pH (acidic versus basic). Bacterial killing efficiency of **(D)** PDA-Pep (Van) and **(E)** PDA-Pep (AMP) at different pH (acidic versus basic). PDA-Pep concentration: 10 mg/mL. The concentrations of Van and AMP encapsulated in the gels are 10 μM and 20 μM, respectively.

bacteria that remained in the culture. Based on the plate counting results, PDA-Pep (Van) exhibited potent antimicrobial activity towards *MRSA* at pH 7.5 and 8.5 with ~70% and ~99% bacterial killing efficiency, respectively (Fig. 3D). In contrast, the antimicrobial activity of PDA-Pep (Van) was much lower in the acidic bacterial culture, with killing efficiency at ~20% and ~25% at pH 5.5 and pH 6.5, respectively. A similar trend of pH-dependent antimicrobial activity against *MRSA* was observed for PDA-Pep (AMP) (Fig. 3E). PDA-Pep (AMP) showed the highest killing efficiency at ~ 90% against *MRSA* at pH 8.5 while it exhibited a moderate to weak antimicrobial activity at a neutral or acidic culture. It is noteworthy that Van and AMP alone exhibited comparable bacterial killing efficiency at all pH conditions (Fig. S9). Thus, the pH-dependent antimicrobial activity of PDA-Pep hydrogels is largely caused by the pH-triggered drug release to kill bacteria. The fluorescence live/dead assay was performed to further confirm alkaline-triggered antibacterial activity. Bacteria were seeded on a glass slide overnight followed by deposition of hydrogels on top of the bacterial colonies. Upon incubation for 4 h, bacteria were stained with live/dead assay kit for fluorescence imaging. Live bacteria show green fluorescence and dead bacteria exhibit red fluorescence. As shown in Fig. 4, PDA-Pep alone did not exhibit antimicrobial activity against *MRSA* at all pH conditions. PDA-Pep (Van) and PDA-Pep (AMP) exhibited pH-dependent antimicrobial activity with predominant dead bacteria shown in red under both the neutral and alkaline conditions. While most bacteria were viable in the acidic culture, the majority of bacteria were killed in the alkaline culture upon hydrogel treatment. The hemocompatibility of PDA-Pep with and without antimicrobials was also evaluated. PDA-Pep, PDA-Pep (Van) and PDA-Pep (AMP) hydrogels prepared at 10 mg/mL were incubated with human red blood cells (HRBCs) at three different pHs for 4 h and the released hemoglobin was quantified by UV—Vis spectroscopy. As shown in Fig. S10, gels under all pH conditions demonstrated good hemocompatibility with less than 10% of hemolysis using Triton-100 as the positive control.

### 3.6. Translational potential of PDA-Pep hydrogels as alkaline-responsive theranostic antimicrobial materials

As a preliminary effort to assess the translational potential of the PDA-Pep hydrogels, we tested the antimicrobial activity and colorimetric response of the gels toward bacteria that are cultured under different pH conditions and later inoculated on pig skins. PDA-Pep (Van) hydrogels were applied on top of the inoculation sites and incubated at 37 °C for qualitative, real-time monitoring of the color change of gels and bacterial killing efficiency. As shown in Fig. 5, gels that are deposited on acidic bacteria at pH 5.5 and 6.5 largely remained blue within the 2 h testing time window. A blue-to-purple colorimetric transition was observed for gels in contact with bacteria at increased pH values. Based on the visual inspection, such transition occurred in ~1 h at a pH of 7.5 and less than 0.5 h at a pH of 8.5. The residual bacteria on the pig skins were thoroughly washed off into culture media which were then subject to a serial dilution for plate counting of the viable *MRSA* bacteria upon hydrogel treatment at different pH conditions. Bacterial killing efficiency was calculated as the ratio of the CFU of bacteria treated with PDA-Pep (Van) to that of PDA-Pep hydrogels without antibiotics. As shown in Fig. 5B, a substantially higher bacterial killing efficiency (73.71%) was observed for gels at a pH of 8.5 followed by 63.90% at pH 7.5 while gels under the acidic condition

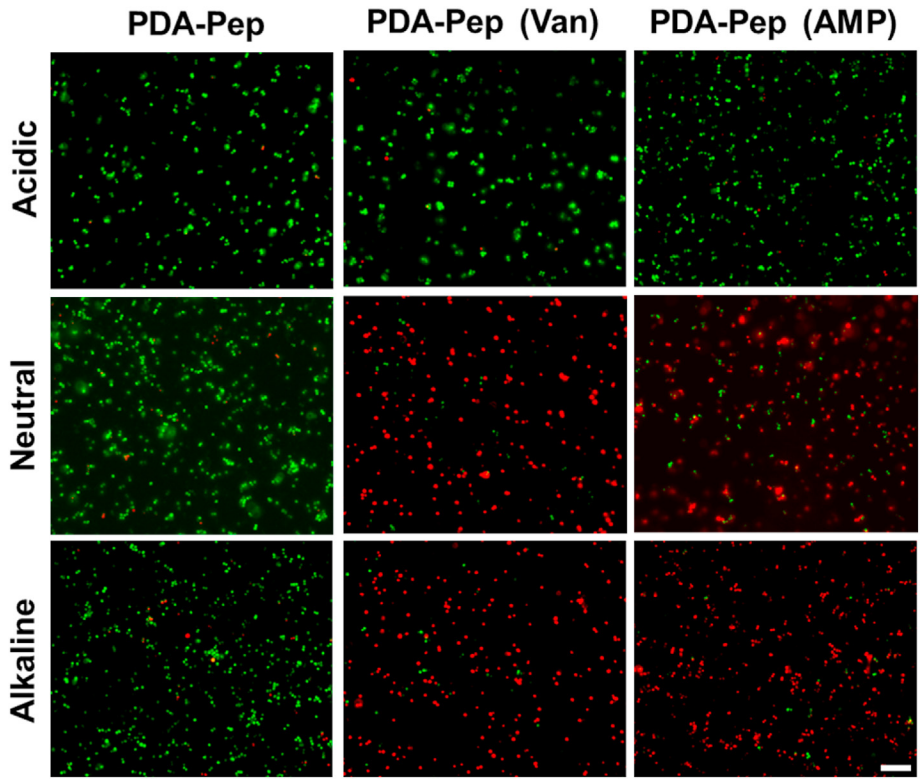


**Fig. 4.** Fluorescence live/dead assay images of *MRSA* treated with PDA-Pep, PDA-Pep (Van) and PDA-Pep (AMP) at the acidic condition (pH 5.5), neutral condition (pH 7.5) and alkaline condition (pH 8.5). PDA-Pep concentration: 10 mg/mL. The concentrations of Van and AMP encapsulated in the gel are 10 μM and 20 μM, respectively. Scale bar: 20 μm.

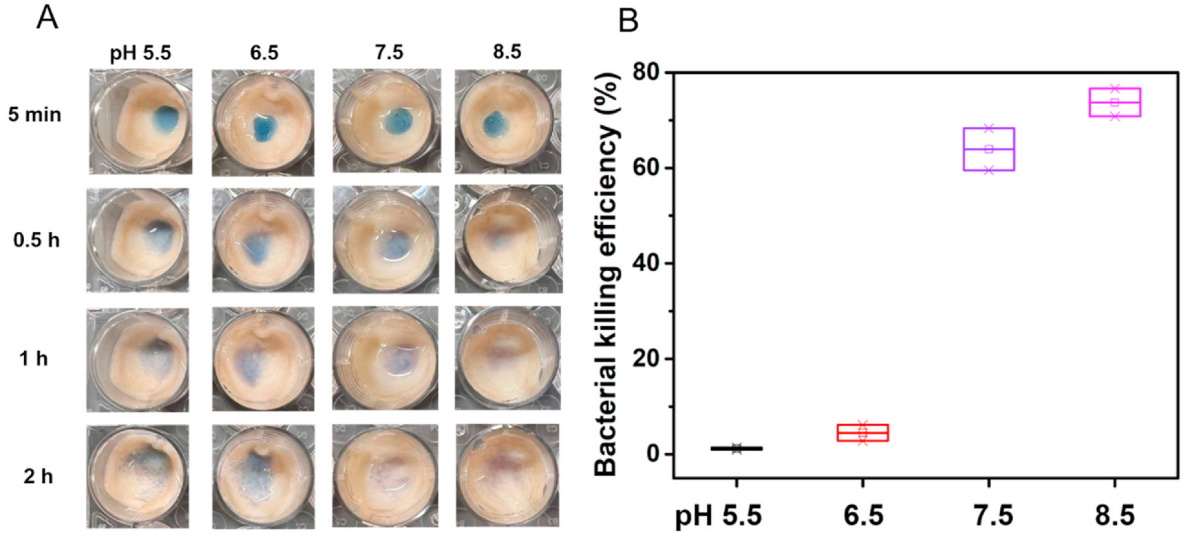


**Fig. 5.** (**A**) Real-time monitoring of the colorimetric transition of the PDA-Pep (Van) hydrogel that are applied on top of the inoculated bacteria on pig skins. (**B**) Bacterial killing efficiency of PDA-Pep (Van) hydrogel at different pH conditions toward inoculated bacteria on pig skins. PDA-Pep concentration: 10 mg/mL. The concentration of Van encapsulated in the gel is 10 μM.

have minimal antimicrobial activity with 1.21% (pH 5.5) and 4.50% (pH 6.5) killing efficiency. Taken together, the PDA-Pep (Van) hydrogels showed potent alkaline-triggered antimicrobial activity, easy-to-read colorimetric transition and good hemocompatibility. These properties highlight their great potential as theranostic materials for real-time monitoring and on-demand treatment of bacterial infections with increased alkalinity.

## 4. Conclusions

In summary, we demonstrated the design, synthesis and alkalinity-induced antimicrobial activity of PDA-Pep hydrogels. The increase of the local bacterial pH triggers a conformational change response within the PDA domain leading to a blue-to-purple colorimetric transition. Simultaneously, a gel-to-sol phase transition occurs causing the release of antibiotics or antimicrobial

peptides into the site of infection. PDA-Pep systems are not only promising sensors; this first-time study demonstrates their ability as functional antimicrobial hydrogels. PDA-Peps achieve real-time monitoring of the local alkaline pH changes in bacterial infections and simultaneously trigger antimicrobial drug delivery. The work shown here represents our initial efforts in building this material framework. Future studies are focused on the application of these materials toward infection treatment associated with an alkaline bacterial microenvironment, for example diseases involving chronic wound infections and others.

## Data availability

The processed data required to reproduce the findings in this work can be shared through personal request.

## Credit author statement

Weike Chen: Conceptualization, Methodology, Investigation, Visualization, Writing – original draft. Shan Hazoor: Methodology, Investigation, Writing – review & editing. Ryan Madigan: Investigation. Ashley. A. Adones: Investigation. Uday. K. Chintapula: Investigation. Kytai T. Nguyen: Methodology, Supervision, Writing – review & editing. Liping Tang: Methodology, Supervision, Writing – review & editing. Frank W. Foss Jr.: Methodology, Supervision, Writing – review & editing. He Dong: Conceptualization, Methodology, Supervision, Writing – review & editing, Project administration, Funding acquisition.

## Declaration of competing interest

The authors declare that they have no known competing financial interests or personal relationships that could have appeared to influence the work reported in this paper.

## Acknowledgments

This study was supported by the National Science Foundation (W.C., H.D. by DMR1824614; F.F. by CMI2004111), the National Institute of Health (U.K.C., K.T.N. by NIH R15 HL156076), the Welch Foundation (S.H. by Y-2031-20200401) and the start-up fund from the University of Texas at Arlington.

## Appendix A. Supplementary data

Supplementary data to this article can be found online at https://doi.org/10.1016/j.mtadv.2022.100288.

## References

[1] X. Wang, M. Shan, S. Zhang, X. Chen, W. Liu, J. Chen, X. Liu, Stimuli-responsive antibacterial materials: molecular structures, design principles, and biomedical applications, Adv. Sci. 9 (13) (2022), 2104843.
[2] A. Sikder, A. Chaudhuri, S. Mondal, N.D.P. Singh, Recent advances on stimuli-responsive combination therapy against multidrug-resistant bacteria and biofilm, ACS Appl. Bio Mater. 4 (6) (2021) 4667–4683.
[3] L.-L. Li, H.-L. Ma, G.-B. Qi, D. Zhang, F. Yu, Z. Hu, H. Wang, Pathological-condition-driven construction of supramolecular nanoassemblies for bacterial infection detection, Adv. Mater. 28 (2) (2016) 254–262.
[4] Q. Lin, J.M. Pilewski, Y.P. Di, Acidic microenvironment determines antibiotic susceptibility and biofilm formation of *pseudomonas aeruginosa*, Front. Microbiol. 12 (2021).
[5] H. Vu, A. Nair, L. Tran, S. Pal, J. Senkowsky, W. Hu, L. Tang, A device to predict short-term healing outcome of chronic wounds, Adv. Wound Care 9 (6) (2019) 312–324.
[6] W. Chen, S. Li, P. Renick, S. Yang, N. Pandy, C. Boutte, K.T. Nguyen, L. Tang, H. Dong, Bacterial acidity-triggered antimicrobial activity of self-assembling peptide nanofibers, J. Mater. Chem. B 7 (18) (2019) 2915–2919.
[7] M. Xiong, Y. Bao, X. Xu, H. Wang, Z. Han, Z. Wang, Y. Liu, S. Huang, Z. Song, J. Chen, R.M. Peek, L. Yin, L.-F. Chen, J. Cheng, Selective killing of *Helicobacter pylori* with pH-responsive helix-coil conformation transitionable antimicrobial polypeptides, Proc. Natl. Acad. Sci. U.S.A. 114 (48) (2017) 12675–12680.
[8] A.F. Radovic-Moreno, T.K. Lu, V.A. Puscasu, C.J. Yoon, R. Langer, O.C. Farokhzad, Surface charge-switching polymeric nanoparticles for bacterial cell wall-targeted delivery of antibiotics, ACS Nano 6 (5) (2012) 4279–4287.
[9] M.H. Kathawala, W.L. Ng, D. Liu, M.W. Naing, W.Y. Yeong, K.L. Spiller, M. Van Dyke, K.W. Ng, Healing of chronic wounds: an update of recent developments and future possibilities, Tissue Eng. B Rev. 25 (5) (2019) 429–444.
[10] L.A. Schneider, A. Korber, S. Grabbe, J. Dissemond, Influence of pH on wound-healing: a new perspective for wound-therapy? Arch. Dermatol. Res. 298 (9) (2007) 413–420.
[11] S. Itoyama, E. Noda, S. Takamatsu, J. Kondo, R. Kawaguchi, M. Shimosaka, T. Fukuoka, D. Motooka, S. Nakamura, M. Tanemura, Enterococcus spp. have higher fitness for survival, in a pH-dependent manner, in pancreatic juice among duodenal bacterial flora, JGH Open 6 (1) (2022) 85–90.
[12] P. Melamed, F. Melamed, Chronic metabolic acidosis destroys pancreas, J. Pancreas 15 (6) (2014) 552–560.
[13] S. Milo, N.T. Thet, D. Liu, J. Nzakizwanayo, B.V. Jones, A.T.A. Jenkins, An in-situ infection detection sensor coating for urinary catheters, Biosens. Bioelectron. 81 (2016) 166–172.
[14] S. Shrestha, J. Wu, B. Sah, A. Vanasse, L.N. Cooper, L. Ma, G. Li, H. Zheng, W. Chen, M.P. Antosh, X-ray induced photodynamic therapy with copper-cysteamine nanoparticles in mice tumors, Proc. Natl. Acad. Sci. U.S.A. 116 (34) (2019) 16823–16828.
[15] C. Ma, C. Li, D. Jiang, X. Gao, J. Han, N. Xu, Q. Wu, G. Nie, W. Chen, F. Lin, Screening of a specific peptide binding to esophageal squamous carcinoma cells from phage displayed peptide library, Mol. Cell. Probes 29 (3) (2015) 182–189.
[16] L. Lin, L. Xiong, Y. Wen, S. Lei, X. Deng, Z. Liu, W. Chen, X. Miao, Active targeting of nano-photosensitizer delivery systems for photodynamic therapy of cancer stem cells, J. Biomed. Nanotechnol. 11 (4) (2015) 531–554.
[17] J. Zhou, M. Duan, D. Huang, H. Shao, Y. Zhou, Y. Fan, Label-free visible colorimetric biosensor for detection of multiple pathogenic bacteria based on engineered polydiacetylene liposomes, J. Colloid Interface Sci. 606 (2022) 1684–1694.
[18] S. Hussain, R. Deb, S. Suklabaidya, D. Bhattacharjee, S. Arshad Hussain, Polydiacetylene a unique material to design biosensors, Mater. Today Proc. 65 (5) (2022) 2765–2772.
[19] A. Kumar, S. Sivagnanam, S. Ghosh, P. Das, Polydiacetylene (PDA) liposome-based colorimetric sensor for the detection of ATP in aqueous medium, Mater. Today Proc. 40 (2021) S230–S235.
[20] C. Kim, K. Lee, Polydiacetylene (PDA) liposome-based immunosensor for the detection of exosomes, Biomacromolecules 20 (9) (2019) 3392–3398.
[21] J.P. Yapor, A. Alharby, C. Gentry-Weeks, M.M. Reynolds, A.K.M.M. Alam, Y.V. Li, Polydiacetylene nanofiber composites as a colorimetric sensor responding to *escherichia coli* and pH, ACS Omega 2 (10) (2017) 7334–7342.
[22] J. Park, S.K. Ku, D. Seo, K. Hur, H. Jeon, D. Shvartsman, H.-K. Seok, D.J. Mooney, K. Lee, Label-free bacterial detection using polydiacetylene liposomes, Chem. Commun. 52 (68) (2016) 10346–10349.
[23] N. Tran, P. Shiveshwarkar, J. Jaworski, Peptide linked diacetylene amphiphiles for detection of epitope specific antibodies, Chemosensors 10 (2) (2022) 62.
[24] H.A.M. Ardoña, J.D. Tovar, Peptide π-electron conjugates: organic electronics for biology? Bioconjugate Chem. 26 (12) (2015) 2290–2302.
[25] S.R. Diegelmann, N. Hartman, N. Markovic, J.D. Tovar, Synthesis and alignment of discrete polydiacetylene-peptide nanostructures, J. Am. Chem. Soc. 134 (4) (2012) 2028–2031.
[26] J. Jaworski, K. Yokoyama, C. Zueger, W.-J. Chung, S.-W. Lee, A. Majumdar, Polydiacetylene incorporated with peptide receptors for the detection of trinitrotoluene explosives, Langmuir 27 (6) (2011) 3180–3187.
[27] L. Hsu, G.L. Cvetanovich, S.I. Stupp, Peptide amphiphile nanofibers with conjugated polydiacetylene backbones in their core, J. Am. Chem. Soc. 130 (12) (2008) 3892–3899.
[28] E.L. Bakota, O. Sensoy, B. Ozgur, M. Sayar, J.D. Hartgerink, Self-assembling multidomain peptide fibers with aromatic cores, Biomacromolecules 14 (5) (2013) 1370–1378.
[29] H. Dong, S.E. Paramonov, L. Aulisa, E.L. Bakota, J.D. Hartgerink, Self-assembly of multidomain peptides: balancing molecular frustration controls conformation and nanostructure, J. Am. Chem. Soc. 129 (41) (2007) 12468–12472.
[30] S. Chae, J.P. Lee, J.M. Kim, Mechanically drawable thermochromic and mechanothermochromic polydiacetylene sensors, Adv. Funct. Mater. 26 (11) (2016) 1769–1776.
[31] S.-Y. Kuo, H.-H. Li, P.-J. Wu, C.-P. Chen, Y.-C. Huang, Y.-H. Chan, Dual colorimetric and fluorescent sensor based on semiconducting polymer dots for ratiometric detection of lead ions in living cells, Anal. Chem. 87 (9) (2015) 4765–4771.
[32] I.S. Park, H.J. Park, J.-M. Kim, A soluble, low-temperature thermochromic and chemically reactive polydiacetylene, ACS Appl. Mater. Interfaces 5 (17) (2013) 8805–8812.
[33] S. Huang, H. Yu, Q. Li, Supramolecular chirality transfer toward chiral aggregation: asymmetric hierarchical self-assembly, Adv. Sci. 8 (8) (2021), 2002132.
[34] P. Duan, H. Cao, L. Zhang, M. Liu, Gelation induced supramolecular chirality:

chirality transfer, amplification and application, Soft Matter 10 (30) (2014) 5428–5448.
[35] G.P. Volynets, F. Barthels, S.J. Hammerschmidt, O.V. Moshynets, S.S. Lukashov, S.A. Starosyla, H.V. Vyshniakova, O.S. Iungin, V.G. Bdzhola, A.O. Prykhod'ko, Identification of novel small-molecular inhibitors of *Staphylococcus aureus* sortase A using hybrid virtual screening, J. Antibiot. 75 (6) (2022) 321–332.
[36] J. Wang, H. Li, J. Pan, J. Dong, X. Zhou, X. Niu, X. Deng, Oligopeptide targeting sortase a as potential anti-infective therapy for *Staphylococcus aureus*, Front. Microbiol. 9 (2018) 245.